Assessing ^{18}F-FDG Uptake in the Sentinel Lymph Node in Breast Cancer

Ismet Sarikaya[1] and Ali Sarikaya[2]

[1]*Department of Nuclear Medicine, Kuwait University Faculty of Medicine, Mubarak Al-Kabeer Hospital, Kuwait City, Kuwait; and*
[2]*Department of Nuclear Medicine, Trakya University Faculty of Medicine, Edirne, Turkey*

^{18}F-FDG PET/CT has limited value in early breast cancer. Sentinel lymph node (SLN) biopsy is the current procedure of choice to search for small metastatic deposits in the axillary lymph nodes in early breast cancer. In this retrospective study, we reevaluated ^{18}F-FDG PET/CT images after locating the SLN on PET/CT with the help of SLN SPECT/CT images and assessed ^{18}F-FDG uptake, particularly in the SLN. Our goal was to understand if combined evaluation of ^{18}F-FDG PET/CT and SLN SPECT/CT could be useful for detecting early lymph node metastasis in the axilla. **Methods:** ^{18}F-FDG PET/CT images of newly diagnosed breast cancer patients who also had SLN scintigraphy (SPECT/CT) and biopsy results were analyzed to assess ^{18}F-FDG uptake in the SLN. The SLN seen on SPECT/CT images was located on PET/CT images, and its metabolic activity was assessed both visually and semiquantitatively using SUV_{max}. ^{18}F-FDG PET results were compared with the histopathology result for the SLN. **Results:** Twenty patients among 130 met the inclusion criteria. SLN SPECT/CT images were helpful for locating the SLN on ^{18}F-FDG PET/CT images in all 20 patients. Histopathologic analysis of the SLNs demonstrated metastasis in 7 patients and no metastasis in 13. There was mild (visible) ^{18}F-FDG uptake in the SLN (SUV_{max}, 1.2–4.1; metastatic deposit size, 6–8 mm) in 6 of 7 patients with SLN metastasis (85.7%). There was no or only faint ^{18}F-FDG uptake in the SLN ($SUV_{max} < 1$) in 9 of 13 patients with no SLN metastasis (69.2%). Receiver-operating-characteristic curve analysis indicated that the SUV_{max} cutoff for differentiating SLN-positive from -negative cases was 0.85 (sensitivity, 85.7%; specificity, 61.5%; area under the curve, 0.747; $P < 0.05$). **Conclusion:** Combined evaluation of ^{18}F-FDG PET/CT and SPECT/CT images to assess ^{18}F-FDG uptake, particularly in the SLN, is a new image analysis technique to detect early metastatic disease in the axillary lymph nodes in breast cancer. Although this technique does not currently seem feasible for use in routine practice, mainly because of the limitations of current PET/CT technology in detecting small tumors, it is an interesting image analysis technique to be aware of for possible future use.

Key Words: breast cancer; sentinel lymph node; ^{18}F-FDG; PET/CT; SPECT/CT

J Nucl Med Technol 2019; 47:149–153
DOI: 10.2967/jnmt.118.219758

Received Aug. 30, 2018; revision accepted Oct. 3, 2018.
For correspondence or reprints contact: Ismet Sarikaya, Department of Nuclear Medicine, Faculty of Medicine, Kuwait University, P.O. Box 24923, Safat, Kuwait 13110.
E-mail: isarikaya99@yahoo.com
Published online Nov. 9, 2018.
COPYRIGHT © 2019 by the Society of Nuclear Medicine and Molecular Imaging.

PET/CT performed with ^{18}F-FDG is commonly used for staging of locally advanced noninflammatory and inflammatory breast cancer (*1–6*). Locally advanced breast cancer (tumor > 5 cm or involving regional lymph nodes or adjacent tissues such as skin, muscle, or bones) includes clinical stages IIB, IIIA, IIIB, and IIIC. Invasive ductal carcinoma is the most common subtype of breast cancer, and invasive lobular carcinoma is the second most common (*7*). Invasive ductal carcinoma shows higher ^{18}F-FDG uptake than invasive lobular carcinoma of the breast (*8–10*). Inflammatory breast cancer is rare but aggressive and involves rapidly proliferating tumor. Inflammatory breast cancer is classified as T4d, and the skin over the breast is reddened, warm, and thickened, termed *peau d'orange* (*11*).

^{18}F-FDG PET/CT is not recommended for the initial assessment of patients with clinical T1 N0 (tumor < 2–3 cm with no lymph node metastasis) breast cancer (*3*). In early breast cancer, sentinel lymph node (SLN) biopsy is routinely used to search for occult lymph node metastasis (*12,13*). The SLN is the lymph node that receives initial lymphatic drainage from the tumor site. The SLN biopsy procedure includes peritumoral or periareolar radiopharmaceutical injection (with or without imaging) or blue dye injection shortly before the surgery, searching for the most radioactive lymph nodes using a handheld γ-probe or blue nodes, surgical sampling, and frozen-section evaluation of the SLN (*14*). If there is metastasis in the SLN in frozen sections, the surgeon proceeds with axillary dissection. Standard axillary dissection is limited to levels I and II, and at least 10 lymph nodes are removed. If there is metastatic disease in the level II nodes, level III nodes may also be removed (complete axillary dissection).

In most of the ^{18}F-FDG PET imaging studies that are done in locally advanced breast cancer, there is regional lymph node metastasis with or without distant metastasis. In some patients, mild ^{18}F-FDG uptake is seen in the axillary lymph nodes in addition to the primary tumor, and such findings are usually reported as negative or insignificant for lymph node metastasis. In those cases, SLN scintigraphy and biopsy are performed to localize the SLN and search for occult axillary lymph node metastasis.

In this retrospective study, we reevaluated ^{18}F-FDG PET/CT images after locating the SLN on PET/CT with the help

of SLN SPECT/CT images and assessed ^{18}F-FDG uptake, particularly in the SLN. Our goal was to understand if combined evaluation of ^{18}F-FDG PET/CT and SLN SPECT/CT could be useful for detecting early lymph node metastasis in the axilla.

MATERIALS AND METHODS

In this retrospective study, newly diagnosed breast cancer patients who had undergone both ^{18}F-FDG PET/CT and SLN SPECT/CT and for whom biopsy results were available for the SLN were selected for further analysis. In all cases, SNL scintigraphy was performed after ^{18}F-FDG PET/CT imaging had been found negative for metastatic disease. This retrospective study was approved by the Kuwait Ministry of Health.

^{18}F-FDG PET/CT images were obtained on a Gemini time-of-flight PET/CT camera (Philips) 60 min after intravenous injection of 296 MBq (8 mCi) of ^{18}F-FDG. Before PET image acquisition, a low-dose CT scan was obtained for attenuation correction and anatomic localization. The PET acquisition was at a rate of 3 min per bed position from the top of the head to the mid thighs. PET images were corrected for attenuation on the basis of the CT data, reconstructed using a standard iterative algorithm (ordered-subset expectation maximization), and reformatted into transaxial, coronal, and sagittal views. Maximum-intensity projections were also generated. Both attenuation-corrected and uncorrected PET images, as well as PET/CT images, were reviewed.

SLN scintigraphic images were obtained on a Discovery 670 16-slice SPECT/CT camera (GE Healthcare) after periareolar intradermal injections of ^{99m}Tc-nanocolloid at 4 sites (3-, 6-, 9-, and 12-o'clock) using a 27-G needle with a dose of 18.5–37 MBq (0.5–1.0 mCi) divided into 4 parts, each in a 0.1- to 0.2-mL volume. In our department, we first obtain dynamic images over the anterior chest/axilla, at 30 s per image for 20 min. This is followed by a static image of 5 min and a SPECT/CT acquisition at 20–25 s/projection, 120 or 128 projections over 360°, with a matrix size of 128 × 128. CT is low-dose (140 kVp and 2.5 mA).

SLNs were identified on dynamic, static, and SPECT/CT images. The SLN seen on the SPECT/CT image was located on the ^{18}F-FDG PET/CT image, and its metabolic activity was assessed visually and using SUV_{max}. Whole-body ^{18}F-FDG PET images were also reviewed to assess the primary tumor, both axilla and breasts, and the rest of the body.

The data were managed and statistically analyzed using the Statistical Package for Social Sciences, version 25.0. The mean ± SD of the ^{18}F-FDG SUV_{max} of tumor-positive and -negative SLNs was calculated. The mean values were compared using the nonparametric Mann–Whitney test. A 2-tailed P value of less than 0.05 was considered statistically significant.

We also performed receiver-operating-curve (ROC) analysis to determine the optimal cutoff for SUV_{max} in SLN-positive and SLN-negative cases.

RESULTS

Images of 20 women (mean age, 61.2 y; range, 35–81 y) were selected for further analysis among 130 patients with newly diagnosed breast cancer. Fifteen patients had invasive ductal carcinoma, 2 had invasive lobular carcinoma, 1 had invasive mammary carcinoma, 1 had ductal carcinoma in situ, and 1 had both invasive ductal carcinoma and invasive lobular carcinoma in the same breast. There were bilateral tumors in 2 patients.

TABLE 1
Histologic Subtype, Tumor Grade, Pathologic Stage, ^{18}F-FDG Uptake in SLN, and Pathology Result

Age (y)	Subtype	Grade	Stage	SLN SUV_{max}	SLN metastasis
53	IDC	2	pT1c N1a Mx	1.2	Positive
35	IDC	3	pT2 N2a Mx	1.5	Positive
74	IDC	2	pT2 N1a Mx	0.8	Positive
45	IDC	2	pT2 N1a Mx	4.1	Positive
53	IDC	2	pT3 N2a Mx	2.8	Positive
67	IDC	2	pT2 N1a Mx	2	Positive
50	ILC (left)*	2	pT3 N3a Mx	–	–
	ILC (right)	2	pT1c N3a Mx	1.4	Positive
47	IDC	2	pT2 N0 Mx	1.4	Negative
62	IDC	3	pT2 N0(sln) Mx	0.9	Negative
61	IDC	2	pT2 N0(sln) Mx	0.6	Negative
70	IDC	2	pT2 N0 Mx	0.8	Negative
68	IDC	3	pT2 N0 Mx	5.9	Negative
49	IDC	2	pT1a N0(sln) Mx	1.8	Negative
78	IDC	1	pT2p N0(sln) Mx	0.8	Negative
68	IDC	2	pT2 N0(sln) Mx	0.9	Negative
53	IDC	1	pT1c N0(sln) Mx	0.7	Negative
76	DCIS	NA	Bilateral	0.9	Negative
70	ILC and IDC	3 and 2	pmT2 N0(sln) Mx	0.9	Negative
81	ILC	2	pT1c N0 Mx	0.8	Negative
65	IMC	3	pT1c N0(sln)	1.8	Negative

*SLN study not done for left breast.

IDC = invasive ductal carcinoma; DCIS = ductal carcinoma in situ; ILC = invasive lobular carcinoma; NA = not applicable; IMC = invasive mammary carcinoma.

SLN scintigraphy was able to localize the SLN in all patients. The number of the SLNs detected by scintigraphy was 1 in 13 patients and 2 or more in 7 patients.

Surgery included SLN biopsy in all patients, with lumpectomy or wide local excision in 9, mastectomy in 11, and axillary dissection or clearance in 10.

SLN SPECT/CT images were helpful in locating the SLN on ^{18}F-FDG PET/CT images in all 20 patients. Table 1 shows histologic subtype, grade, pathologic stage, ^{18}F-FDG uptake (SUV_{max}) of SLN, and pathology result of SLN. SLN biopsy and histopathology demonstrated metastasis in 7 patients and no metastasis in 13 patients. There was mild visible ^{18}F-FDG uptake in the SLN in 6 of 7 patients with SLN metastasis (SUV_{max}, 1.2–4.1; metastatic deposit size, 6–8 mm) (Fig. 1). In 1 patient with SLN metastasis, there was only faint ^{18}F-FDG uptake in the SLN (SUV_{max}, 0.8; metastatic deposit size, 3 mm). In 4 patients with SLN metastasis, there was bilateral axillary node uptake, which was milder on the nontumoral side in 3 and equal on both sides in 1. In addition to uptake in the SLN, there was also mild ^{18}F-FDG uptake in several other axillary nodes on the tumor side in 3 patients who had both sentinel and nonsentinel node metastatic disease on histopathology.

In 9 of 13 patients with no SLN metastasis on histopathology, there was no or faint ^{18}F-FDG uptake in the SLN ($SUV_{max} < 1$) (Fig. 2). There was mild ^{18}F-FDG uptake in the SLN in 4 of 13 patients with no SLN metastasis (SUV_{max}, 1.4–5.9). In a patient with prominent ^{18}F-FDG uptake in the SLNs (SUV_{max}, 5.9), the SLNs were located in level III on SPECT/CT. It was not clear if axillary dissection included level III nodes in this patient. There was bilateral mild axillary uptake in 5 patients who were negative for SLN metastasis; this finding was to a similar degree on both sides in 4 patients and less intense on the nontumoral side in 1 patient.

The mean ± SD for ^{18}F-FDG SUV_{max} in SLN-positive and -negative cases was 2.06 ± 1.21 and 1.4 ± 1.35, respectively. Statistically, there was no significant difference in the values ($P = 0.08$).

ROC analysis indicated that the SUV_{max} cutoff for differentiating SLN-positive from SLN-negative cases was 0.85. The sensitivity of this value was 85.7% (95% confidence interval, 83.1−88.4), and the specificity was 61.5% (95% confidence interval, 59.7–63.6), with an area under the curve of 0.747 ($P < 0.05$). Figure 3 shows the ROC curve.

There were several foci of abnormal ^{18}F-FDG uptake in the spine that were suggestive of bone metastasis in a patient with grade 3 invasive ductal carcinoma, pathologic stage pT2 N2a Mx, and mild focal ^{18}F-FDG uptake in the SLN and several other axillary nodes.

DISCUSSION

Detection of early metastatic disease in the regional lymph nodes is important for the selection of appropriate treatment and improving survival. SLN biopsy is the current method to search for small amounts of metastatic deposits in the axillary lymph nodes in early breast cancer. Micrometastasis includes tumors measuring 0.2–2 mm or more than 200 cells. Macrometastasis is when the tumor is larger than 2 mm. Intraoperative frozen sections of SLNs have a low sensitivity in detecting micrometastases but a reasonable sensitivity for macrometastases (*15,16*). ^{18}F-FDG PET imaging can detect metastatic deposits larger than 6–8 mm.

In routine ^{18}F-FDG PET studies, mild uptake ($SUV_{max} < 2.5$) in the axillary lymph nodes is usually reported as negative or insignificant for metastatic disease and considered to be due to inflammatory changes. In the current study, we assessed ^{18}F-FDG PET uptake particularly in the SLN. SLN SPECT/CT images were helpful in locating the SLN and assessing ^{18}F-FDG uptake in the SLN. SPECT/CT is becoming increasingly available, and the CT part of the study is useful to determine the exact anatomic location of the SLNs.

We did not find a statistically significant difference in ^{18}F-FDG SUV_{max} between tumor-positive and tumor-negative

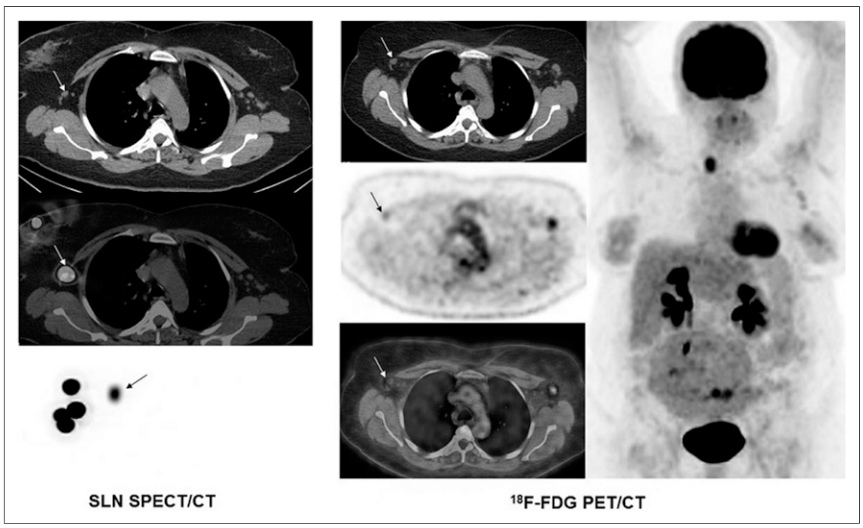

FIGURE 1. A 50-y-old woman with bilateral grade 2 invasive lobular carcinoma (left breast, pT3 N3a Mx; right breast, pT1c N3a Mx). (Left) SLN scintigraphic study from right breast with selected transaxial CT, SPECT/CT, and maximum-intensity-projection images demonstrates SLN in right axilla (arrows). (Middle) Selected ^{18}F-FDG transaxial PET, CT, and PET/CT images of bilateral axillae demonstrate mild focal uptake in SLN in right axilla (SUV_{max}, 1.4) (arrows) and multiple mildly hypermetabolic left axillary lymph nodes (SUV_{max}, 2.9). Histopathologic analysis demonstrated metastasis in right SLN and bilaterally in multiple axillary lymph nodes. (Right) ^{18}F-FDG PET whole-body maximum-intensity-projection image demonstrates bilateral diffuse uptake in breasts, focal mild tumoral uptake in left breast (SUV_{max}, 2.3), and bilateral mildly hypermetabolic axillary lymph nodes, more prominent on left side. Abnormal hypermetabolic activity in right lobe of thyroid is suspicious for malignancy and large myomatous uterus is also seen.

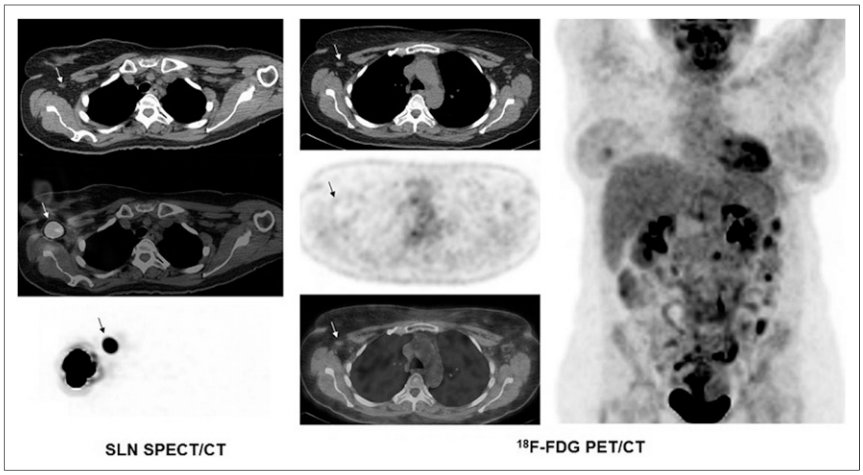

FIGURE 2. A 53-y-old woman with grade 1 invasive ductal carcinoma of right breast (pT1c N0(sln) Mx). (Left) SLN scintigraphic study from right breast with selected SPECT/CT and maximum-intensity-projection images demonstrates SLN in right axilla (arrows). (Middle) Selected ^{18}F-FDG transaxial PET, CT, and PET/CT images demonstrate only faint uptake in SLN in right axilla (SUV_{max}, 0.7) (arrows). Mild but slightly more prominent ^{18}F-FDG uptake is seen in contralateral left axillary lymph nodes. Histopathologic analysis demonstrated no evidence of metastasis in right SLN. (Right) ^{18}F-FDG PET whole-body maximum-intensity-projection image demonstrates bilateral diffuse uptake in breasts and focal tumoral uptake in right breast (SUV_{max}, 2.1).

SLNs. The absence of a difference in SUV_{max} between SLN-positive and SLN-negative patients was probably related to the small sample size and to the generally low uptake in lymph nodes. However, in most of our patients with SLN metastasis, there was visible mild focal uptake in the SLN (86%). Mild visible focal uptake in the SLN was seen in a lesser percentage of patients with no SLN metastasis (31%). The SUV_{max} of mild but visible focal uptake ranged from 1.2 to 4.1 in SLN-positive patients. In cases with faint ^{18}F-FDG uptake in the SLN in SLN-negative patients, SUV_{max} was less than 1. ROC analysis showed that the SUV_{max} cutoff was 0.85 in differentiating SLN-positive from SLN-negative cases. However, given the small number of patients in our study, the accuracy of ROC analysis is limited. Bilateral mild axillary uptake was of equal intensity in most SLN-negative cases and was more prominent on the tumor side in SLN-positive patients. It is already well known that bilateral symmetric lymph node uptake is likely due to a benign process, such as inflammatory conditions, and asymmetric uptake is more suspected of indicating metastatic disease in oncologic cases. Mild visible focal uptake in axillary lymph nodes, if unilateral or more prominent on the tumor side, raises suspicion of early metastatic disease. If the abnormal uptake is only in the SLN but not in other nodes, this may further raise suspicion for early lymph node metastasis even if the SUV_{max} is less than 2.5. However, it is still difficult to decide if mild ^{18}F-FDG uptake in the SLN is due to a small amount of metastatic disease or to inflammatory changes. SLN biopsy is still the procedure of choice to detect early metastatic disease in the SLN.

Histopathologically determined sizes of the metastatic deposits were 6–8 mm in our 6 cases with mild focal ^{18}F-FDG uptake in the SLN. In a case with a metastatic deposit size of 3 mm, ^{18}F-FDG PET was negative. It is well known that ^{18}F-FDG PET imaging is limited in detecting small metastatic deposits (<6 mm). The physical size of a lesion is difficult to derive from PET images because of spill-out and partial-volume effects (*17,18*). The smaller the tumor, the greater the underestimation of the uptake via PET imaging (*17,18*). Different tumors with exactly the same uptake value or phantoms with same radioactivity concentrations in different-sized spheres show that uptake decreases when tumor or sphere size decreases (*17,19*). In recent years, there have been various attempts to improve small lesion detection, including time-of-flight PET cameras, PET cameras with solid-state photodetectors, digital PET, point-spread function (PSF) reconstruction, and reconstruction with smaller voxels (*20–25*). Recent studies have demonstrated that PSF reconstruction improves detection of small metastatic deposits in various cancers (*26–29*). PSF reconstruction can improve spatial resolution and signal-to-noise ratio in PET imaging (*18*). In breast cancer patients, PET with PSF reconstruction performed better than PET with ordered-subset expectation maximization reconstruction in detecting nodal metastases 7 mm or smaller, and the smallest detectable metastasis was 1.8 mm (*26*). The reconstruction of PET images with time-of-flight and PSF enabled the improvement of diagnostic

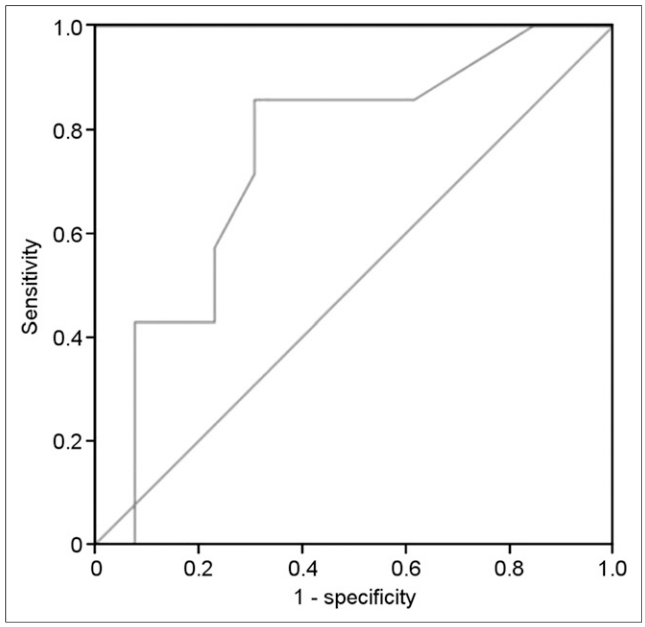

FIGURE 3. ROC curve for ^{18}F-FDG PET/CT in detecting metastasis in SLN.

performance in N-staging of breast carcinoma, even when the dose of radiopharmaceutical was reduced to 2.5 MBq/kg (*27*). In our cases, we used iterative or ordered-subset expectation maximization reconstruction. PSF reconstruction may help better detect ^{18}F-FDG uptake in the SLN with a small amount of metastatic disease. PSF reconstruction improves detection of small deposits, but Munk et al. reported that PSF reconstruction artifacts can lead to misinterpretations when used for quantitative analyses of small subcentimeter lesions, which is important when monitoring treatment response on lymph nodes using SUV measurements (*18*).

Because of the current limitations of PET/CT imaging for detecting small tumor deposits, obtaining both ^{18}F-FDG PET/CT and SLN SPECT/CT in early breast cancer is currently not feasible in routine use. Obtaining both images is costly and time-consuming and increases radiation dose. However, it is important to combine different techniques and imaging modalities to obtain the maximum available result for a study.

CONCLUSION

Combined evaluation of ^{18}F-FDG PET/CT and SLN SPECT/CT images allows assessing ^{18}F-FDG uptake, particularly in the SLN, which is important in detecting early lymph node metastasis in breast cancer. Although this technique does not seem feasible in routine practice, mainly because of the limitations of current PET/CT technology in detecting small amounts of tumor, it is an interesting image analysis technique to be aware of for possible future use.

DISCLOSURE

No potential conflict of interest relevant to this article was reported.

ACKNOWLEDGMENT

We thank Dr. Galip Ekuklu for his help in statistical analysis.

REFERENCES

1. Lee JH. Radionuclide methods for breast cancer staging. *Semin Nucl Med.* 2013;43:294–298.
2. Caresia Aroztegui AP, García Vicente AM, Alvarez Ruiz S, et al.; Oncology Task Force of the Spanish Society of Nuclear Medicine and Molecular Imaging. ^{18}F-FDG PET/CT in breast cancer: evidence-based recommendations in initial staging. *Tumour Biol.* 2017;39:1010428317728285.
3. Groheux D, Cochet A, Humbert O, et al. ^{18}F-FDG PET/CT for staging and restaging of breast cancer. *J Nucl Med.* 2016;57(suppl 1)17S–26S.
4. Carkaci S, Macapinlac HA, Cristofanilli M, et al. Retrospective study of ^{18}F-FDG PET/CT in the diagnosis of inflammatory breast cancer: preliminary data. *J Nucl Med.* 2009;50:231–238.
5. Alberini JL, Lerebours F, Wartski M, et al. ^{18}F-fluorodeoxyglucose positron emission tomography/computed tomography (FDG-PET/CT) imaging in the staging and prognosis of inflammatory breast cancer. *Cancer.* 2009;115:5038–5047.
6. Groheux D, Giacchetti S, Delord M, et al. ^{18}F-FDG PET/CT in staging patients with locally advanced or inflammatory breast cancer: comparison to conventional staging. *J Nucl Med.* 2013;54:5–11.
7. Barroso-Sousa R, Metzger-Filho O. Differences between invasive lobular and invasive ductal carcinoma of the breast: results and therapeutic implications. *Ther Adv Med Oncol.* 2016;8:261–266.
8. Avril N, Rosé CA, Schelling M, et al. Breast imaging with positron emission tomography and fluorine-18 fluorodeoxyglucose: use and limitations. *J Clin Oncol.* 2000;18:3495–3502.
9. Gil-Rendo A, Martínez-Regueira F, Zornoza G, et al. Association between [^{18}F] fluorodeoxyglucose uptake and prognostic parameters in breast cancer. *Br J Surg.* 2009;96:166–170.
10. Groheux D, Giacchetti S, Moretti J-L, et al. Correlation of high ^{18}F-FDG uptake to clinical, pathological and biological prognostic factors in breast cancer. *Eur J Nucl Med Mol Imaging.* 2011;38:426–435.
11. van Uden DJ, van Laarhoven HW, Westenberg AH, de Wilt JH, Blanken-Peeters CF. Inflammatory breast cancer: an overview. *Crit Rev Oncol Hematol.* 2015;93:116–126.
12. Zahoor S, Haji A, Battoo A, et al. Sentinel lymph node biopsy in breast cancer: a clinical review and update. *J Breast Cancer.* 2017;20:217–227.
13. De Cicco C, Cremonesi M, Luini A, et al. Lymphoscintigraphy and radioguided biopsy of the sentinel axillary node in breast cancer. *J Nucl Med.* 1998;39:2080–2084.
14. Giammarile F, Alazraki N, Aarsvold JN, et al. The EANM and SNMMI practice guideline for lymphoscintigraphy and sentinel node localization in breast cancer. *Eur J Nucl Med Mol Imaging.* 2013;40:1932–1947.
15. Lombardi A, Nigri G, Maggi S, et al. Role of frozen section in sentinel lymph node biopsy for breast cancer in the era of the ACOSOG Z0011 and IBCSG 23-10 trials. *Surgeon.* 2018;16:232–236.
16. Liu LC, Lang JE, Lu Y, et al. Intraoperative frozen section analysis of sentinel lymph nodes in breast cancer patients: a meta-analysis and single-institution experience. *Cancer.* 2011;117:250–258.
17. Soret M, Bacharach SL, Buvat I. Partial-volume effect in PET tumor imaging. *J Nucl Med.* 2007;48:932–945.
18. Munk OL, Tolbod LP, Hansen SB, Bogsrud TV. Point-spread function reconstructed PET images of sub-centimeter lesions are not quantitative. *EJNMMI Phys.* 2017;4:5.
19. Hoffman EJ, Huang SC, Phelps ME. Quantitation in positron emission computed tomography, 1: effect of object size. *J Comput Assist Tomogr.* 1979;3:299–308.
20. van der Vos CS, Koopman D, Rijnsdorp S, et al. Quantification, improvement, and harmonization of small lesion detection with state-of-the-art PET. *Eur J Nucl Med Mol Imaging.* 2017;44:4–16.
21. Vandenberghe S, Mikhaylova E, D'Hoe E, Mollet P, Karp JS. Recent developments in time-of-flight PET. *EJNMMI Phys.* 2016;3:3.
22. Cherry SR, Sorenson JA, Phelps ME. *Physics in Nuclear Medicine.* 4th ed. Philadelphia, PA: Elsevier/Saunders; 2012.
23. Koopman D, van Dalen JA, Lagerweij MC, et al. Improving the detection of small lesions using a state-of-the-art time-of-flight PET/CT system and small voxel reconstructions. *J Nucl Med Technol.* 2015;43:21–27.
24. Nguyen NC, Vercher-Conejero JL, Sattar A, et al. Image quality and diagnostic performance of a digital PET prototype in patients with oncologic diseases: initial experience and comparison with analog PET. *J Nucl Med.* 2015;56:1378–1385.
25. Slomka PJ, Pan T, Germano G. Recent advances and future progress in PET instrumentation. *Semin Nucl Med.* 2016;46:5–19.
26. Bellevre D, Blanc Fournier C, Switsers O, et al. Staging the axilla in breast cancer patients with ^{18}F-FDG PET: how small are the metastases that we can detect with new generation clinical PET systems? *Eur J Nucl Med Mol Imaging.* 2014;41:1103–1112.
27. Ferdová E, Baxa J, Ňaršanská A, et al. Low-dose high-resolution 18F-FDG-PET/CT using time-of-flight and point-spread function reconstructions: a role in the detection of breast carcinoma axillary lymph node metastases. *Anticancer Res.* 2018;38:4145–4148.
28. Lasnon C, Hicks RJ, Beauregard JM, et al. Impact of point spread function reconstruction on thoracic lymph node staging with ^{18}F-FDG PET/CT in non-small cell lung cancer. *Clin Nucl Med.* 2012;37:971–976.
29. Hotta M, Minamimoto R, Yano H, Gohda Y, Shuno Y. Diagnostic performance of ^{18}F-FDG PET/CT using point spread function reconstruction on initial staging of rectal cancer: a comparison study with conventional PET/CT and pelvic MRI. *Cancer Imaging.* 2018;18:4.